Proceedings of ICFDP9:
Ninth International Congress of Fluid Dynamics & Propulsion
December 18-21, 2008, Alexandria, Egypt

ICFDP9-EG-258

Study of Unguided Flow in a Chamber

A. Abdel- Fattah

Associate professor, Department of Mechanical Power Engineering, Faculty of Engineering Minoufiya University, Shebin El-Kom, Egypt.
ashourabdelfatah@yahoo.com

ABSTRACT

In the present, a steady laminar of two dimensional and incompressible fluid flow induces from wall injection in a circular chamber has been studied experimentally and numerically. The water is injected from injection system into the chamber through the wall jets. The centerline static pressure variation with the distance along the chamber length is measured and calculated at different Reynolds numbers and inlet flow angles. The average heat transfer with Reynolds number at different values of the inlet flow angle is obtained. The velocity vectors are presented and Reynolds number is varied between 433 and 910 with jet angle of 0^o, 15^o, 30^o, 45^o and 60^o. The results indicate that the pressure recovery coefficient decreases as both Reynolds number and flow angle increase. The average heat transfer coefficient increases with increasing both Reynolds number and flow angle. The results showed that two recirculation zones occur in the sides of center line of the chamber behind the step. The size of these recirculation zones decreases by increasing the inlet flow angle. At high value of the inlet flow angle, other recirculation zone occurs on the wall chamber

KEYWORDS: Annular injection, Laminar flow, Two dimensional, Pressure coefficient, Heat transfer

1. INTRODUCTION

Injection using thin lip directed along the wall could be employed to study the flow in combustion chamber. Injection with lip thick or with high angle in the surfaces causes a region of reversed flow.

In the past few decades, the flow problem of the back-facing step and the forward-facing step has been investigated widely. Detailed studies on these problems were reported by Armaly et al. [1]. In this study, the downstream velocity and recirculation sizes a function of Reynolds number were presented. The laminar mixed convection flow over horizontal forward facing step studied experimentally and numerically by Abu-Mulaweh et al. [2]. Their results showed that the length of recirculation regions upstream and downstream of the step was increased as Reynolds number and the step height increase. In another study by Abu-Mulaweh et al. [3], they made an experiment and numerical for laminar natural convection problem for vertical forward facing step. Benchmark results for the back-ward facing step flow problem for Re = 800 are presented by Gartling [4]. Kondoh et al [5] studied the effect of expansion ratio, Reynolds number and Prandtl number. Barton [6] studied the inlet channel effect on the step flow problem. He showed that the primary vortex length was decreased when an upstream channel was presented in the step flow. Carrington and pepper [7] studied the effect of Reynolds number (Re = 400, 800 and 1200) on the recirculation and Vortex zones of the flow in back ward facing step. A steady – state heat transfer for two dimensional laminar, incompressible, plane wall jet over a backward –facing step was carried out by Kanna and Das [8]. They studied the effect of Reynolds number, Prandtl number and step geometry of the heat transfer characteristics. They concluded that, when Reynolds number increases, the isotherms were deflected toward the recirculation region and are concentrated near the wall. Also, when Reynolds number increases, the local Nusselt number along the bottom wall increases to a peak value and is asymptotically reduced in the downstream direction. The control of the isothermal turbulent flow within a rearward- facing step combustor using countercurrent shear was studied experimentally by Forliti and Strykowski [9]. They reported that the use of suction based counter flow is essential to separate mechanisms for achieving shear flow control. First counter flow has an effect of augmenting the natural reverse flow, caused by the sudden expansion of the step. The second mechanism employed using

the counter flow is the modification of the shear layer near the expansion plane. Sea and Parameswaran [10] studied numerically the steady and unsteady flow through a backward facing step. They used the standard k-ε model with standard wall functions to predict buoyancy flow for various Richardson number. Their results showed that, for flow over backward-facing step, buoyancy –driven vortex shedding has been noticed only in the turbulent flow when Richardson number increases to a critical value.

The mean and fluctuating characteristics of a plane unsteady laminar wall jet for constant temperature was investigated by Quintana et al. [11]. Abdel-Fattah [12] studied the effect of wall inclination on the laminar flow characteristics in two dimensional wall jet for the case of entrance uniform flow condition. His results indicated the effect of the wall angle ($\theta = 0^0$, 15^0 ,30^0 and 45^0) on the velocities (u & v) and the pressure (p), the location of maximum velocity of flow and the width of recirculation zone, together with different Reynolds number (50,100 , 500 ,750 and 1000) on these variables .He showed that in the range $0^0 \leq \theta \leq 45^0$, as the wall angle θ^0 increases, the Maximum velocity of flow decays faster, the location of this velocity changes towards free stream, and the jet spreads faster. The width of recirculation zone increases as the wall angle and/or Reynolds number increases.

Kanna and Dos [13] studied the effect of Reynolds number and geometry on the fluid flow of laminar plane offset jet. In addition, Kanna and Dos [14] investigated the conjugate heat transfer from a plane laminar offset jet. They also studied in [15] the conjugate heat transfer of plane wall jet and they reported close form solutions for conjugate interface temperature, local Nusselt number distribution and average Nusselt number.
Manca et al. [16] studied numerically the effect of heated wall position on the mixed convection in channel with an open cavity. Their results are reported in terms of streamlines, isotherms, wall temperature, and velocity profiles in the cavity for Richardson number was 0.1 and 100 and for Reynolds number of 100 and 1000. Their results showed that the maximum temperature values decrease as Reynolds number and Richardson number decrease whereas the effect of the ratio between channel height and cavity height was found to play a significant role on streamline and isotherm patterns for different heating configurations.

The effect of velocity ratio on the turbulent mixing of confined co-axial jets was indicated by Ahmed and Sharma [17] as mean velocity; streamwise and turbulence intensity distributions at different streamwise locations were obtained using laser Doppler velocimeter (LDV) for different values of velocity ratios. Their results indicated that mixing process in confined jets depend strongly not only on the velocity ratio, but also on the interaction between the boundary layer, mixing layer and the main flow, particularly when the area ratio is small.

The present paper focuses on the experimental and numerical study for steady laminar, two dimensional injection flows with variable inlet flow angles in the chamber. The pressure and the heat transfer characteristics are investigated through changing the inlet flow angle and Reynolds number. The velocity vector fields with different inlet flow angles are presented. Finally the numerical results are compared with the experimental results.

2. EXPERIMENTAL SETUP AND MEASURING METHODS

To carry out the experimental work, the apparatus shown in figure (1) is designed. It consists of a centrifugal pump, test section, injection system, supply tank and measuring devices (U-tube differential manometers and thermocouples. The test section is a circular chamber made of commercial steel pipe with diameter 7.62 cm, and length 150 cm. 23 pressure taps of diameter (1 mm) and 12 thermocouples are distributed along the test section for static pressure and temperature measurement, respectively. The injection system shown in figures (1b and 1c) contains the chamber which provides by 12 rectangular slots with different angles to inject hot water. Each rectangular slot has 15 mm length and 2.0 mm width. The required operating flow rate is adjusted using the injected flow pump and control valves. The volume flow rate is measured by the orifice meter which is previously calibrated by collecting tank method.
The static pressure distribution, wall temperature distribution and outlet temperatures are measured. The pressure recovery coefficient is calculated using following equation:

$$C_P = \frac{p - p_{in}}{0.5\rho V_o^2} \qquad (1)$$

Where V_o is the inlet velocity. The total net heat flow, Q, is calculated as follows:

$$Q = \dot{m}\, c_p\, (\bar{t}_{in} - \bar{t}_{out}) \qquad (2)$$

Where $\bar{t}_{in}$ and $\bar{t}_{out}$ are the inlet and outlet temperatures and $\dot{m} = \rho A V_0$ is the mass flow rate and c_p is the specific heat of fluid.
The average heat transfer coefficient h_{av} is evaluated from the following equation:

$$h_{av} = \frac{Q}{A(\bar{t}_b - \bar{t}_w)} \tag{3}$$

Where $\bar{t}_b$ is the fluid mean bulk temperature and $\bar{t}_w$ is the wall mean temperature Then, Nusselt number, Nu, is calculated, based on the hydraulic diameter, as follows:

$$Nu = \frac{h_{av} D}{k_c} \tag{4}$$

Where k_c is thermal conductivity

3. MATHEMATICAL MODELS

The physical model used in this study is shown in figure 1 where two dimensional, incompressible and laminar water flow is considered

Based on the characteristics scales of *D and* V_o, the dimensionless variables are defined as follows.

$$r = \frac{\bar{r}}{D}, \quad z = \frac{\bar{z}}{D}, \quad u = \frac{\bar{u}}{V_o}, \quad v = \frac{v'}{V_o},$$

$$p = \frac{\bar{p}}{0.5\rho V_o^2}, \quad T = \frac{\bar{T}}{\bar{T}_J}, \quad Nu = \frac{h_{av} D}{k_c}$$

Where the over bar represents the dimensional quantities. According to the above assumptions and dimensionless variables, the equations are expressed forms by as the following equations.

Continuity equation

$$\frac{1}{r}\left(\frac{\partial ru}{\partial r} + \frac{\partial rv}{\partial z} \right) = 0 \tag{5}$$

Radial momentum equation:

$$u\frac{\partial u}{\partial r} + v\frac{\partial u}{\partial z} = -\frac{\partial p}{\partial r} + \frac{1}{r}\frac{\partial}{\partial r}\left[r\left(\frac{1}{\mathrm{Re}}\right)\frac{\partial u}{\partial r} \right] + \frac{\partial}{\partial z}\left[\left(\frac{1}{\mathrm{Re}}\right)\frac{\partial u}{\partial z} \right] - \left(\frac{1}{\mathrm{Re}}\right)\frac{2v}{r^2} - \frac{g\,D}{V_o^2} \tag{6}$$

Axial momentum equation:

$$u\frac{\partial v}{\partial r} + v\frac{\partial v}{\partial z} = -\frac{\partial p}{\partial z} + \frac{1}{r}\frac{\partial}{\partial r}\left[r\left(\frac{1}{\mathrm{Re}}\right)\frac{\partial v}{\partial r} \right] + \frac{\partial}{\partial z}\left[\left(\frac{1}{\mathrm{Re}}\right)\frac{\partial v}{\partial z} \right] \tag{7}$$

Energy equation

$$u\frac{\partial T}{\partial r} + v\frac{\partial T}{\partial z} = \frac{1}{r}\frac{\partial}{\partial r}\left[r\left(\frac{1}{\mathrm{Re\ Pr}}\right)\frac{\partial T}{\partial r} \right] + \frac{\partial}{\partial z}\left[\left(\frac{1}{\mathrm{Re\ Pr}}\right)\frac{\partial T}{\partial z} \right] \tag{8}$$

The computational domain boundaries are shown in Fig. (2a). the boundary conditions for the above set of governing equations are as follows:

a) Inlet boundary (a-b) and (c-d)

The uniform velocity profiles are: $v = V_o \cos\theta$, $u = V_o \sin\theta$ and $T=T_J$

b) At walls (b-c, d-e and h-a), the velocity components are zero on the wall.

c) Exit boundary (e-h)

A zero gradient condition is employed for the outlet boundary. Although this boundary condition is strictly valid only when flow is fully developed, it is also permissible for sufficient downstream from the region of interest, i.e,

$$\frac{\partial \phi}{\partial z} = 0 \ and \ \phi = u, v \ and \ T$$

4. SOLUATION PROCEDURE

The mathematical models described above consist of a set of differential equations subject to appropriate boundary conditions. To provide the algebraic form of the governing equations, a fully staggered grid system was adopted for the velocity components and the scalar variables. These equations were discretized using a control volume finite difference method (CVFDM). The numerical solution in the present work is accomplished using Semi- Implicit Method for Pressure Linked Equation (SIMPLE) utilized by Patankar [18]. The velocity component v is calculated at the east and west faces of the main control volumes from the solution of the axial momentum equation. Similarly, the velocity components u at the north and south faces are calculated. When the pressure correction equation is solved, then the velocities and the pressure fields are corrected. To complete iteration, the energy equation is solved. The discretization equations were solved by

the line by line procedure, which is a combination of Gauss-Seidel and tridiagonal matrix algorithm in the stream wise direction. The tridiagonal matrix algorithm (TDMA) was used to solve a set of discretization equations in the cross- stream direction. Relaxation factors were employed to promote smooth convergence of the discretized equations. The relaxation factors were 0.5, 0.5, 0.5 and 0.75 for u, v, p' and T respectively. The converged criterion in this study was based on the successive changes in variables. All field variables were monitored, and the following condition was used to declare convergence:

$$MAX\left|\frac{\phi_{i,j}^{n}-\phi_{i,j}^{n-1}}{\phi_{i,j}^{n}}\right| \le 10^{-4} \qquad (9)$$

In addition, the ratio of the difference between the inlet mass flow rate and the outlet mass flow rate to the inlet mass flow rate was also examined. Convergence was declared if the relative mass imbalance was less than 10^{-3} and Eq. (9) was satisfied simultaneously. After the convergence the flow at this time step**,** the entire variables are taking the initial condition for the new time step. To verify the algorithm, numerical tests were performed to ensure that the solution was grid independent algorithm.

The grid points are distributed uniformly over the computational domain. A ١75 x 85 grid points were placed in the computational domain in Fig. 2(a). Results at a grid independent study are shown in Fig. 2(b)

5. RESULTS AND DISCUSSION

5.1. Mean Flow Vector Fields

Figures 3a-3e illustrate a vector representation of the mean velocity fields for different values of flow angle at Re= 453. In each case, it is clear that the flow issues from the injection proposal to the chamber. The flow spreads toward the downstream direction in the chamber and combining at center line of the chamber. Also, it can be noticed that two recirculation zones are found behind the step between the flows. These recirculation zones depend on the inlet flow angle. Increasing the flow angle causes the size of these recirculation zones to decrease. This is because the radial component increases by increasing the inlet flow angle.

At higher angles ($\theta = 45^{o}$ and 60^{o}) of inlet flow, the size of these recirculation zones becomes smaller and a new recirculation zone can be found between the flow and the wall. This is because the radial component becomes higher than the axial component. (See figures 3d and 3e). Also, the recirculation zones increases as Reynolds number increases (see figures 4a and 4b).

5.2. Effect of Reynolds Number on the Pressure Coefficient.

Figures (5a- 5j) show the pressure coefficient ($\overline{p}-\overline{p}_{in}$ /0.5 ρV_o^2) measured and calculated at the center line of chamber as a function of axial distance (z/L) at different values of the inlet flow angle. Each figure is for two different values of Reynolds number. From these figures, it is seen that, generally, the local pressure coefficient decreases reaching a minimum value due to the recirculation zone behind the step which causes increase of hydraulic losses. Then the local pressure coefficient increases to maximum value at combining point beyond which starts to decrease again gradually in the downstream direction due to the friction effect. Evidently, it shows that the meeting of the flow at the chamber center will result in an increase of the pressure coefficient.

Also, it can be seen that the pressure coefficient decreases by increasing the Reynolds number. This can be explained by the fact that increasing Reynolds number leads to an increase of the hydraulic losses of the flow and also leads to an increase in the kinetic energy which affects of the dimensionless pressure. Also, it is noticed that the peak of the pressure coefficient decreases by increasing Reynolds number. For higher value of injection angle ($\theta = 60^{o}$), it can be seen that the pressure coefficient increases by increasing Reynolds number. The reason for this tendency may be due to the meeting of the flow increases the pressure at higher value of inlet flow angle ($\theta = 60^{o}$). The increment of the pressure is higher the increment of kinetic energy, accordingly the pressure coefficient increases.

5.3. Effect of Inlet Flow Angle on Pressure Coefficient

Figure 6 shows the pressure coefficient ($\overline{p}-\overline{p}_{in}$ /0.5 ρV_o^2) measured and calculated at the center line of chamber as a function of axial distance (z/L) at different values of inlet flow angle and constant value of Reynolds number (Re = 453). From this figure it can be noticed the pressure coefficient before the combining point increases as the inlet flow angle increases. At higher angle ($\theta = 60^{o}$) the pressure coefficient becomes positive values because the length of recirculation zone becomes shorter. Also, the peak of the pressure coefficient moves toward the upstream direction as the flow angle increases. This is because the recirculation zones decrease with increasing the inlet flow angle. In addition, this figure shows that the pressure coefficient after the combining point decreases by increasing the inlet flow angle. The reason for this tendency may be due to the increase of friction loss as the inlet flow angle increases.

5.4. Average Heat Transfer

Overall Nusselt numbers along the chamber are presented in this section to investigate the effect of Reynolds number and the inlet flow angles on the overall heat transfer characteristics.

5.4.1. Effect of Reynolds Number on Nusselt Number

The effect of Reynolds number on Nusselt number is shown in figure 7. The results indicate that, generally Nusselt number increases, due to the increase of Reynolds number for all values of the inlet flow angle. The reason for this tendency may be due to the momentum increases as Reynolds number becomes larger causing an augmentation in the heat transfer coefficient. The numerical results give good agreement with the experimental data.

5.4. 1. Effect of the Inlet Flow Angle on Nusselt Number

Figure 8 presents Nusselt number as a function of the inlet flow angle for two values of Reynolds number of 453 and 630. From this figure, it can be seen that, Nusselt number increases as the inlet flow angle increases. This is because the momentum increases by increasing the inlet flow angle. From this figure, it is seen that the numerical give good agreement with the experimental data.

6. CONCLUSIONS

The behavior of the fluid flow of steady incompressible laminar from the wall injection into the chamber was carried out experimentally and numerically.

The effect of Reynolds number and the inlet flow angle on the pressure recovery coefficient, the heat transfer characteristics and the velocity vector fields are studied. The major conclusion of this research could be summarized as follows:

- Two recirculation zones occur in the sides of chamber center line behind the step. The size of these recirculation zones decreases as the inlet flow angle increases but it increases as Reynolds number increases.
- At high value of inlet flow angle ($\theta = 60^o$), other recirculation zone occurs next to the chamber wall.
- Both the pressure coefficient after the peak value and its peak value at the combining point at the centerline of the chamber decease as inlet flow angle increases but the pressure coefficient increases before the peak value as the inlet angle increases.
- As the inlet flow angle increases, the peak value of pressure at the combining point decreases and shifts in upstream direction. - The comparison between the numerical results and the experimental measurements for pressure gives good agreement
- The value of Nusselt number increases as either Reynolds number or inlet flow angle increases.
- The numerical results is fair with the experimental measurements for average Nusselt number

NOMENCLATURE

Cp	pressure coefficient ($\frac{\overline{p}-\overline{p}_{in}}{0.5\rho V_o^2}$)	
D	hydraulic parameter	m
d_o	orifice diameter	m
h_{av}	average heat transfer coefficient	W/(m^2. K)
k_c	thermal conductivity	W/(m. K)
$\dot{m}$	mass flow rate	kg/sec
Nu	Nusselt number	
Q	input heat	W
P	dimensionless pressure	
$\overline{p}$	static pressure	N/m^2
Re	Reynolds number ($Re=\rho V_o D/\mu$)	
T	dimensionless temperature	
$\overline{T}$	temperature	K ^{o}
u	dimensionless of radial component of local mean velocity ($u=\overline{u}/V_o$)	
$\overline{u}$	radial component of local mean velocity	m/sec
v	dimensionless of axial component of local mean velocity ($v=\overline{v}/V_o$)	
$\overline{v}$	axial component of local mean velocity	m/sec
V_o	inlet mean velocity of slot jet	m/sec
r,z	cylindrical coordinates	

Greeks letters

μ	dynamic viscosity	kg/(m. sec)
ρ	density	kg/m3

Subscripts

av	average
b	bulk
j	jet
in	inlet
o	mean
out	out
T	indices for turbulent
w	wall

REFERENCES

[1] B. F. Armaly, F.Durst, J.C.F.Pereira and B. Schonung, "Experimental and Theoretical Investigation of Backward –
Facing Step Flow", J. Fluid Mech, vol. 127, pp. 473-496,

1983.
[2] HI. Abu-Mulaweh , B.F.Armaly and T.S.Chen, "Measurements of Laminar Mixed Convection Flow Over a Horizontal Forward-Facing Step", Thermophys. Heat Transfer, vol. 7, pp. 569-573, 1993.
[3] HI. Abu-Mulaweh , B.F.Armaly and T.S.Chen, "Laminar Natural Convection Flow over a Vertical Forward-Facing Step", Thermophys. Heat Transfer, vol. 10, pp. 517-523, 1996.
[4] D. K. Gartling ,"A Test Problem for Outflow Boundary Conditions- Flow Over a Backward –Facing Step', Int, J. Numer. Meth. Fluids, vol.11, pp. 953-967, 1990.
[5] T. Kondoh,Y. Nagano and T. Tsuiji, "Computational Study of Laminar Heat Transfer of a Back ward –Facing Step Int, J. Heat Mass Transfer, vol. 36, pp. 577-591, 1993.
[6] L.E. Barton ,"The Entrance Effect of Laminar Flow Over a Back ward –Facing Step Geometry", Int, J. Numeric. Meth. Fluids, vol.25, pp. 633-644, 1997.
[7] D.B.Carrington and D.W. Pepper, "Convective Heat Transfer Downstream of a 3-D Backward-Facing Step", Numerical Heat Transfer Part A. vol.41, (6-7), pp. 555-578, 2002.
[8] P. R. Kanna, M. K. Das," Heat Transfer Study of Two – Dimensional Laminar Incompressible Wall Jet Over Backward –Facing step", Numerical Heat Transfer Part A, Vol. 50, pp. 165- 187, 2006.
[9] D. J. Forliti, P.J. Strykowski, " Controlling Turbulence in a Rearward – Facing Step Combustor Using Countercurrent Shear, Journal of Fluid Engineering, vol. 127, pp. 438-448, 2005.
[10] E. Seo, S. Parameswaran," Numerical Computations of Steady and Unsteady, Separation Buoyant Flows- Part1: Computations with the Standard k-ε Model", Numerical Heat Transfer, Part A, vol. 42, pp. 791- 809, 2002.
[11] D.L. Quintana ,M.Amitay, A. Ortega and I.J. Wygnanski," Heat Transfer in the Forced Laminar Wall Jet, J. Heat Transfer, vol.119, pp. 451-459, 1997.
[12] A. Abdel-Fattah, The Numerical Simulation of the Effect of Wall Inclined on Laminar Flow Characteristics in a Two Dimensional Wall Jet", Engineering Research Journal, Faculty of Eng., Minoufiya Univ., Egypt, vol. 25, pp. 77-93, 2002.
[13] P. R. Kanna, M. K. Das," Numerical Simulation of Two – Dimensional Laminar Incompressible Offset Jet Flows", Int. J. Numerical Meth. Fluids, vol.49, pp. 439-464, 2005.
[14] P. R. Kanna, M. K. Das, Conjugate Heat Transfer Study of Two –Dimensional laminar Incompressible Offset Jet Flows", Int. J. Numerical Heat Transfer Part A, vol. 48, pp. 671-691, 2005.
[15] P. R. Kanna, M. K. Das, "Conjugate Forced Convection Heat Transfer from a Flat Plate by Laminar Plane Wall Jet Flow", Int. J. Heat Mass Transfer, vol. 48, pp. 2896-2910, 2005.
[16] O. Manca , S. Nardini, K. Khanafer , K.Vafai," Effect of Heated Wall Position on Mixed Convection in a Channel with an Open cavity", Numerical Heat Transfer, Part A, vol. 43, pp. (2003) 259-282, 2003.
[17] M.R. Ahmed, S.D. Sharma," Effect of Velocity Ratio on the Turbulent Mixing of Confined, co –Axial Jets, Experimental Thermal and Fluid Science, vol. 22, pp. 19-33, 2000.
[18] S.V. Patankar, "Numerical Heat Transfer and Fluid Flow", McGraw-Hill, New York, 1980

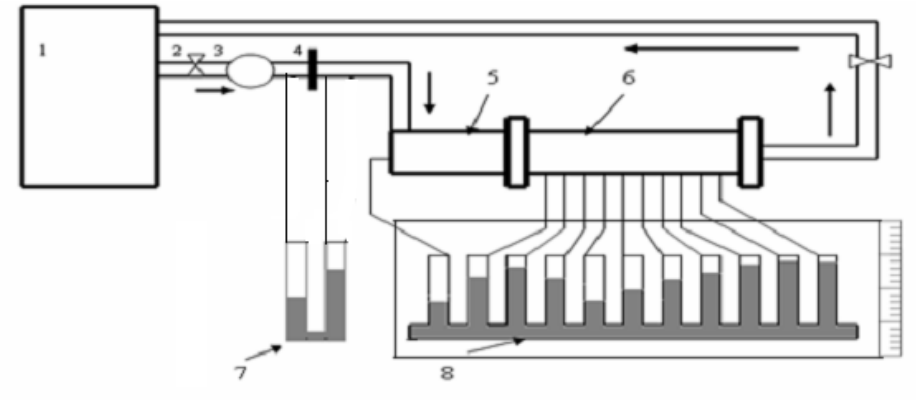

1. Supply tank
2. Control valve
3. Pump
4. Orifice meters
5. Injection system
6. Test section
7 U-tube manometer
8. Bank of U -tube differential manometer

Fig.1a Schematic diagram of experimental apparatus

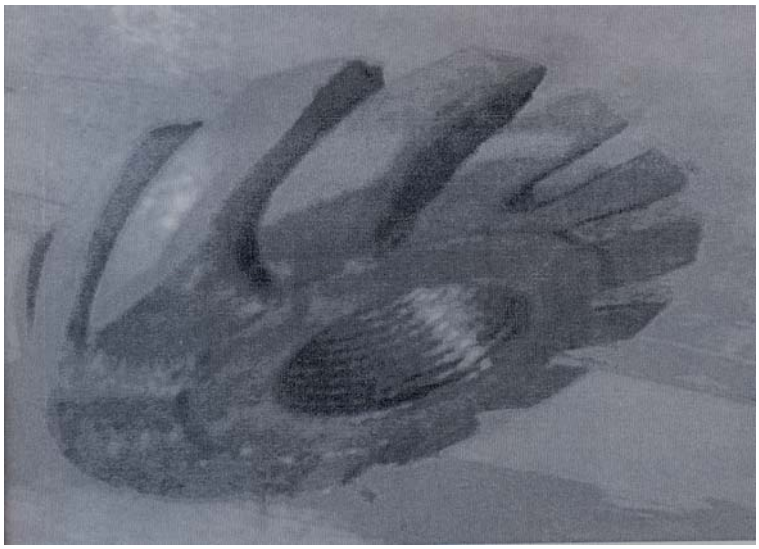

Fig. 1b Flow guide for injection system

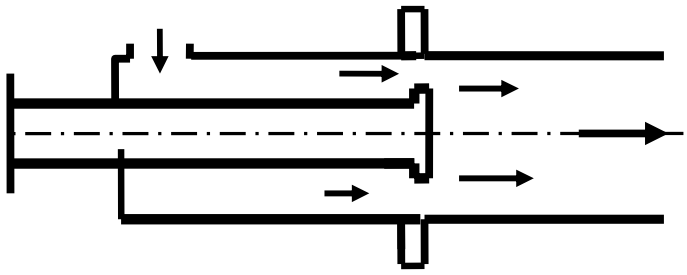

Fig.1c. The injection system

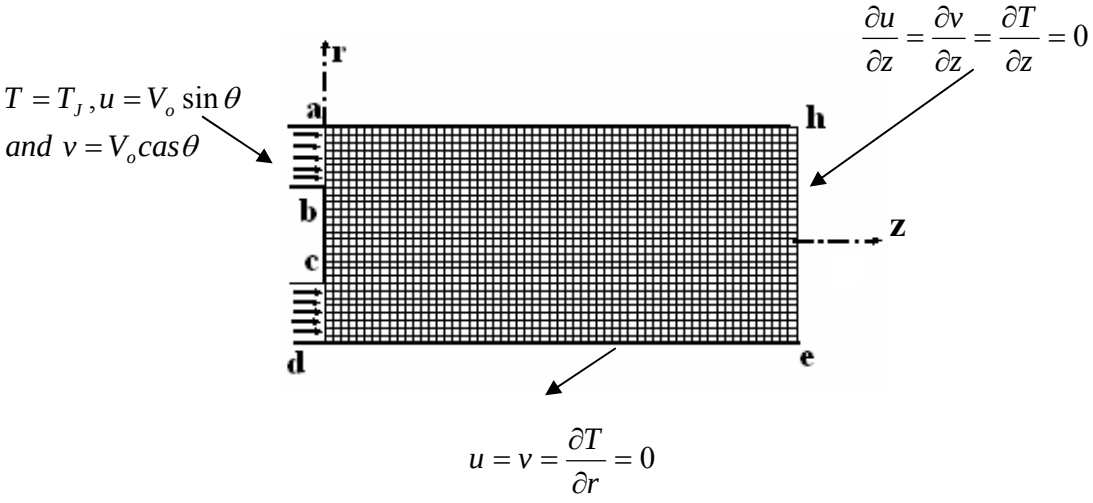

Fig. 2a Computational domain

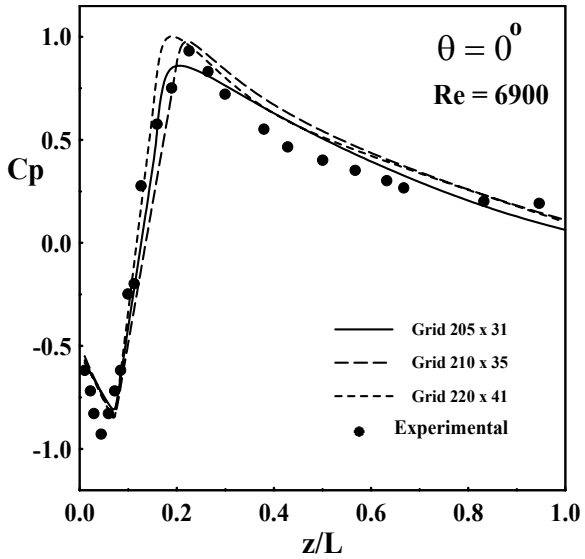

Fig. 2 b Effect of grid refinement on the pressure recovery coefficient

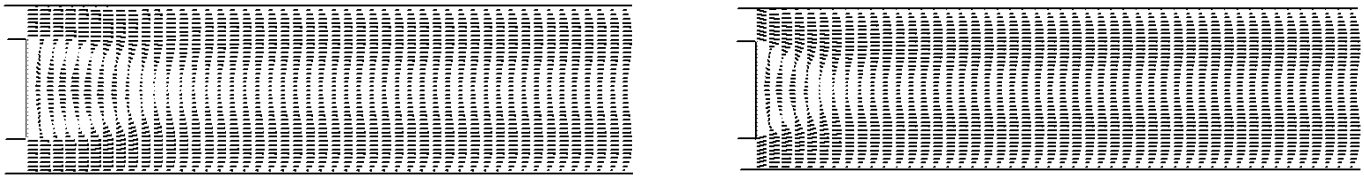

(a) θ = 0° (b) θ = 15°

(c) θ = 30° (d) θ = 45°

(e) θ = 60°

Fig. 3 Mean velocity vector field for different values of inlet flow angle at Re= ٤٥٣

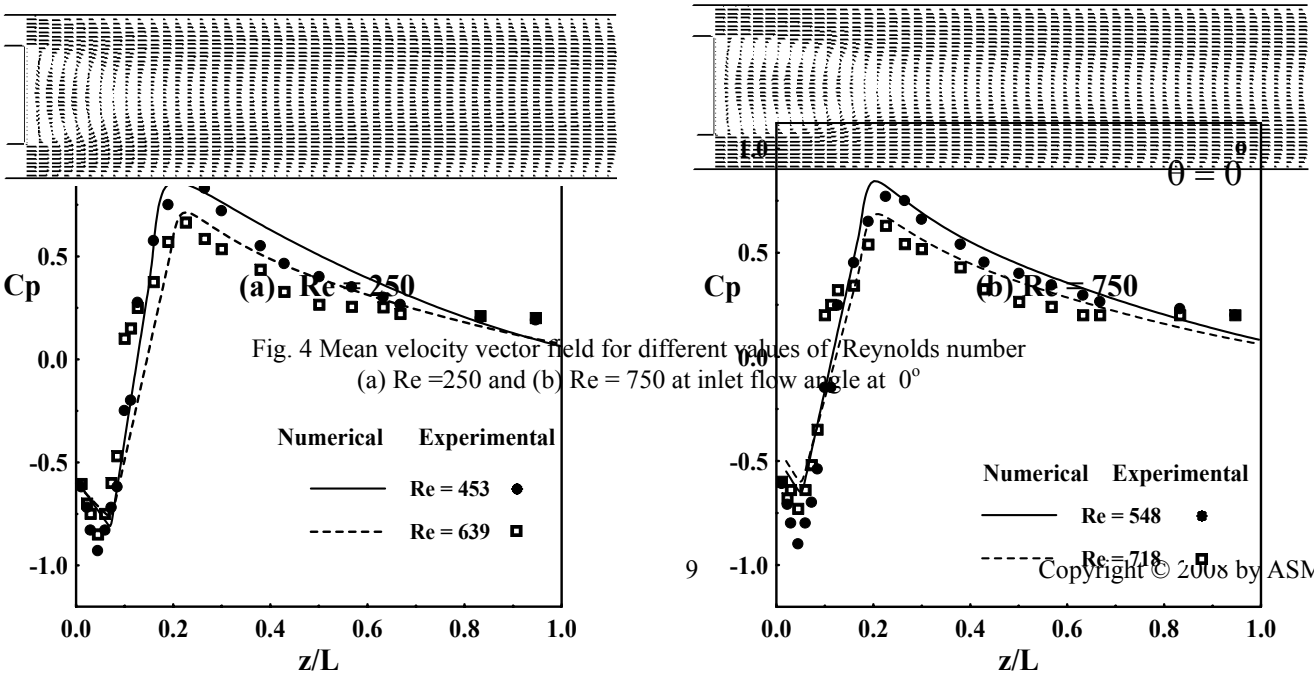

Fig. 4 Mean velocity vector field for different values of Reynolds number (a) Re =250 and (b) Re = 750 at inlet flow angle at 0°

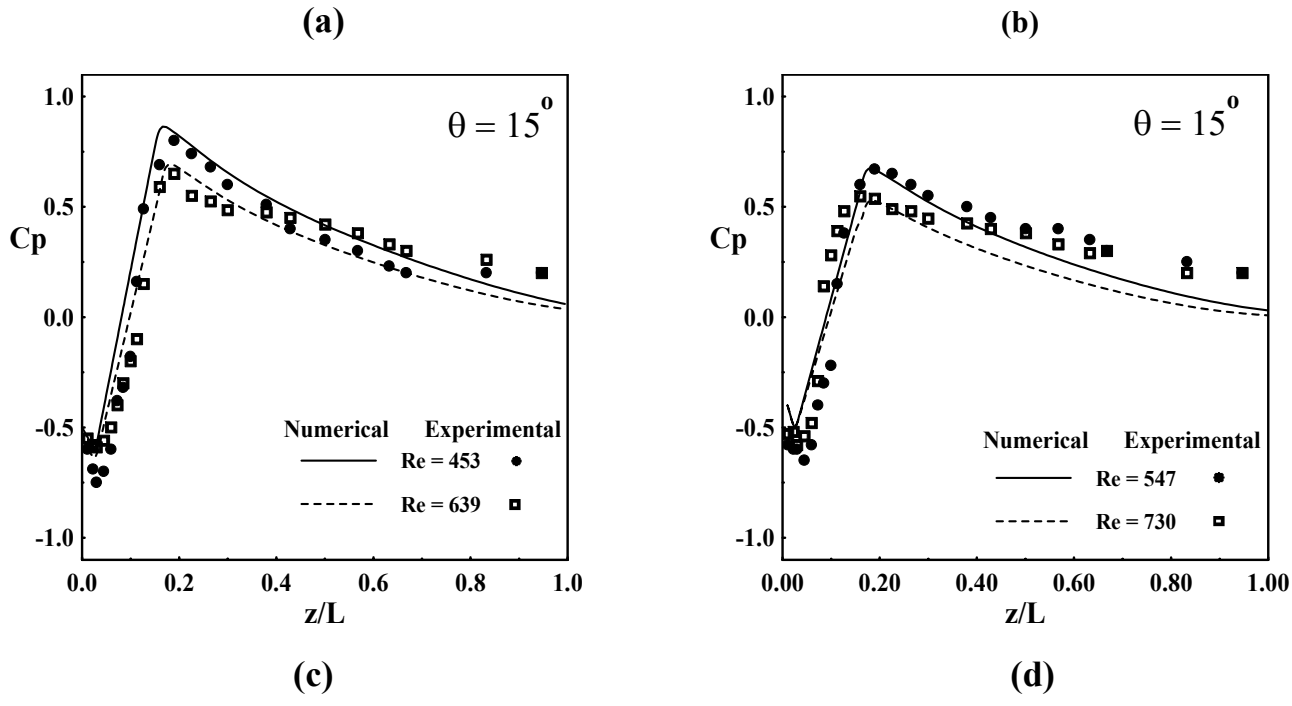

Fig. ◦ Variation of the static pressure along centerline axis of chamber with Reynolds number for inlet flow angle (0^0, 15^o, 30^o, 45^o and 60^o) continued

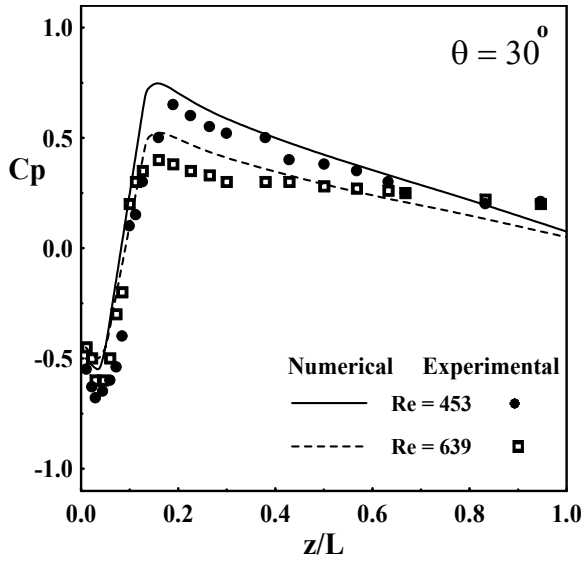

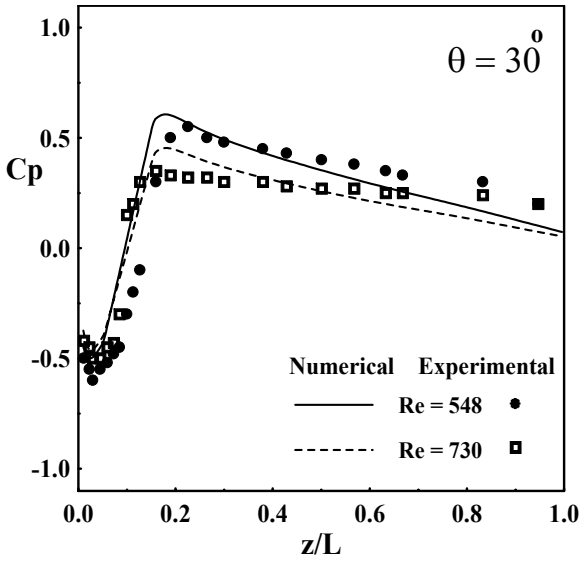

(e)

(f)

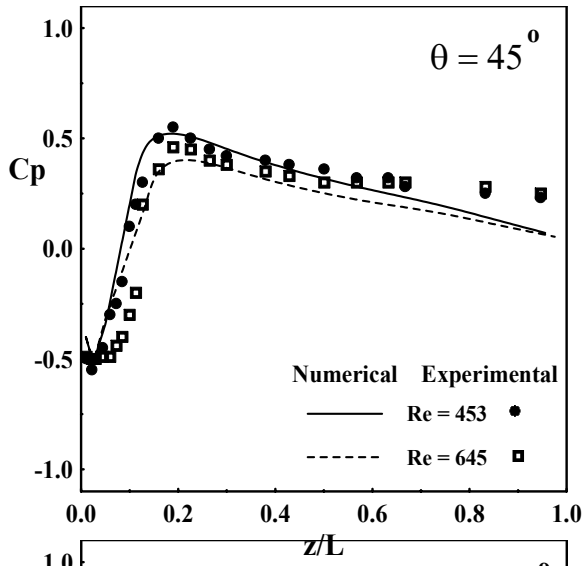

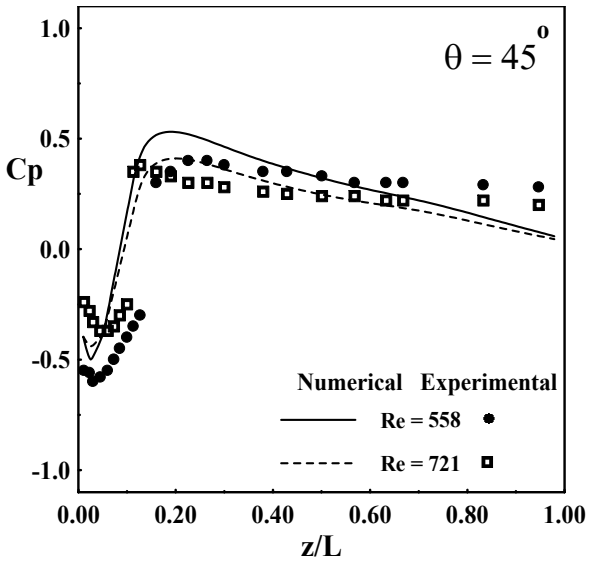

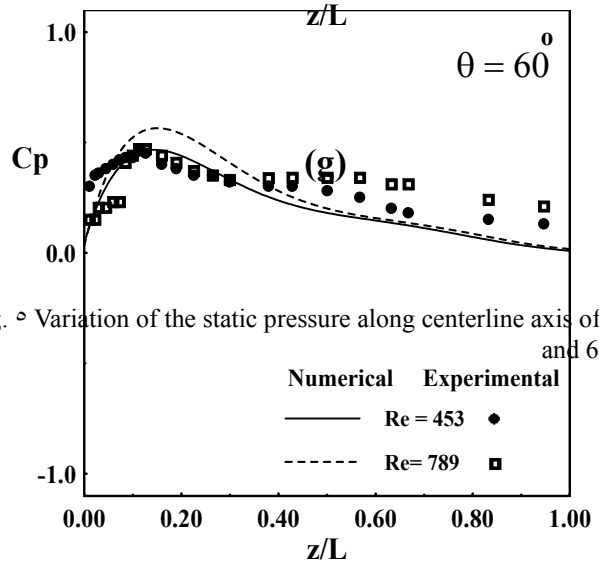

(g)

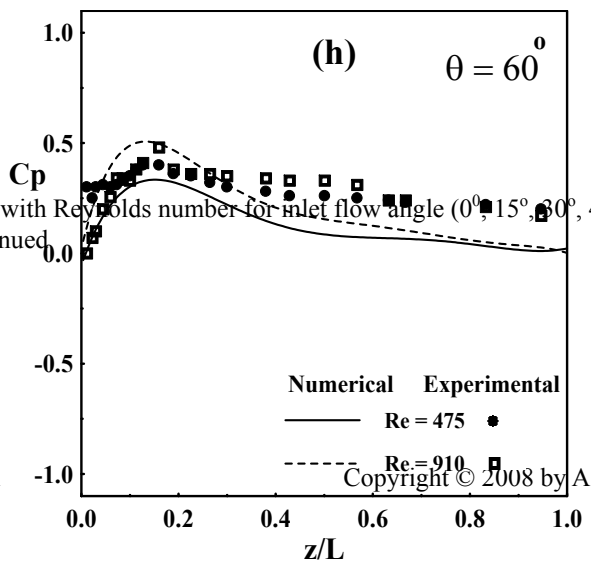

(h)

Fig. ◦ Variation of the static pressure along centerline axis of chamber with Reynolds number for inlet flow angle (0^0, 15^o, 30^o, 45^o and 60^o) continued

(i) (j)

Fig. ∘ Variation of the static pressure along centerline axis of chamber with Reynolds number for inlet flow angle (0^0, 15^o, 30^o, 45^o and 60^o)

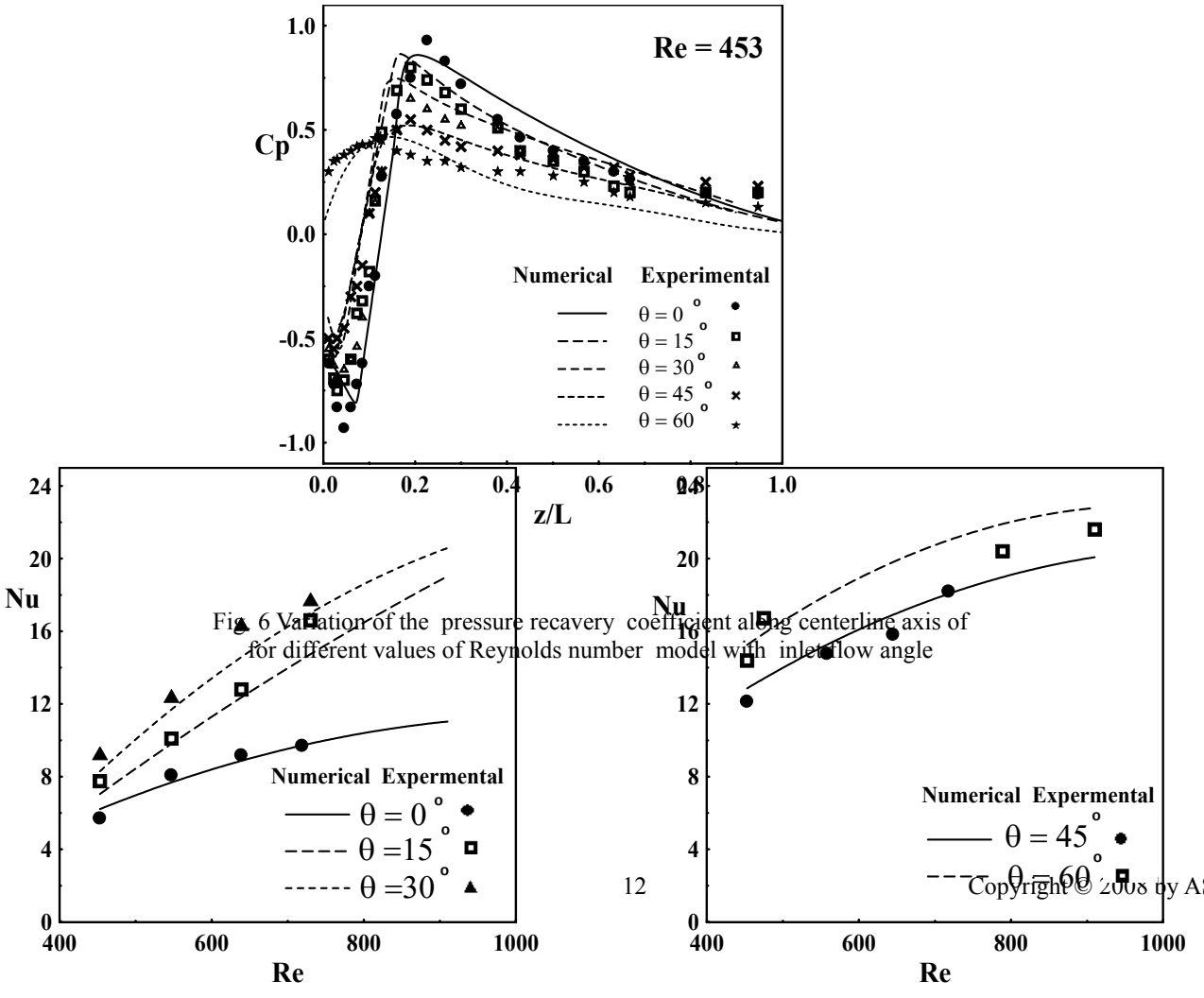

Fig. 6 Variation of the pressure recavery coefficient along centerline axis of for different values of Reynolds number model with inlet flow angle

(a) **(b)**

Fig. 7 Variation of avarge Nusselt number with Reynolds number for inlet flow angle (a) $\theta = 0^o$, 15^o and 30^o and (b) $\theta = 45^o$ and 60^o

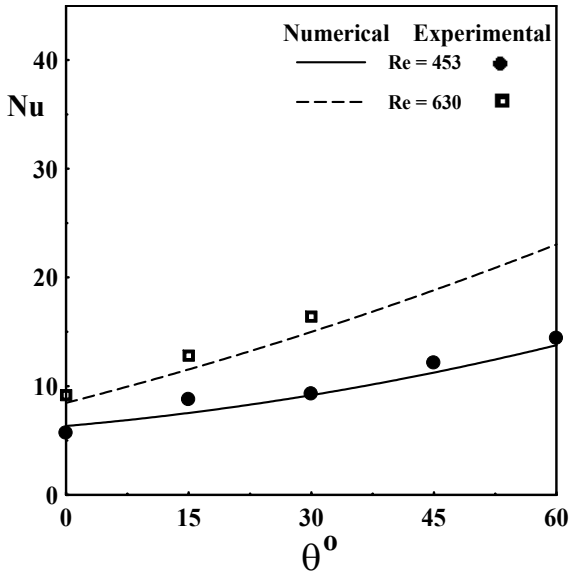

Fig. 8 Variation of avarge Nusselt number with inlet flow angle at Re= 453